Proceedings of the 21st ICSMGE, Vienna, Austria, 14 – 19 June 2026. Pistrol, Adam & Schweiger (eds.)
Published by: ÖGG, Austrian Society for Geomechanics, Salzburg, Austria, ISBN 978-3-9503898-4-5
https://doi.org/10.53243/ICSMGE2026-1906

Investigating Railway Ballast Instability Under Flooding Conditions: A Physical Modeling Approach

Pongsakorn Wongchana, Suchada Wutti, Peerapong Jitsangiam
Department of Civil Engineering, Chiangmai University, Thailand, pongsakorn.w@cmu.ac.th

ABSTRACT: Flooding poses a significant threat to railway infrastructure, often leading to ballast instability that compromises track safety and serviceability. When floodwater overtops and seeps through the ballast layer, concentrated flow between sleeper gaps can accelerate erosion and breach formation. This study investigates the failure mechanisms of sleeper-installed railway ballast under flooding using reduced-scale physical model tests in an open-channel flume at discharge rates of 30 m³/h and 40 m³/h. The results show that higher discharge rates reduce the time to overtopping and significantly intensify ballast displacement. At 30 m³/h, failure progressed through a multi-phase retrogressive collapse, while at 40 m³/h, rapid headcut erosion dominated. Particle Image Velocimetry (PIV) analysis revealed that the higher discharge produced earlier, more widespread, and higher-magnitude particle movement, whereas the lower discharge allowed a slower progression with localized displacement concentrated between sleeper gaps. These findings provide experimental evidence of how hydraulic intensity influences breach evolution in sleeper-installed ballast layers and offer insight for designing flood-resilient railway infrastructure.

KEYWORDS: Railway ballast stability, Flood-induced failure and Physical modeling.

1 INTRODUCTION

Flooding is one of the most frequent and damaging natural hazards affecting railway infrastructure worldwide. In Thailand, the combination of a tropical climate, monsoon rainfall, and increasingly intense extreme weather events results in recurring flood impacts on railway embankments. During severe events, overtopping flows and prolonged inundation can cause ballast displacement, interlocking breakdown, and progressive slope instability, ultimately compromising track safety and serviceability. Historical events, such as the 2011 nationwide floods, have demonstrated the vulnerability of Thailand's rail network, causing extensive service disruptions and infrastructure damage (SRT, 2021).

Railway ballast layers are designed to provide load distribution, maintain track geometry, and facilitate drainage. However, under flooding conditions, high-velocity overtopping flows and seepage can induce breaching—a process involving the removal and transport of ballast particles from the embankment face. This failure mechanism has received limited experimental investigation compared to other flood-induced railway degradation processes such as subgrade settlement, internal erosion, and mud pumping (Liu et al., 2023; Johnston et al., 2024; Zhao et al., 2024).

Insights from hydraulic engineering studies on non-cohesive embankments and landslide dams reveal similar erosion processes, including retrogressive slope collapse, headcut migration, and localized scour under concentrated flows (Li et al., 2021; Zhou et al., 2019; Shen et al., 2022). These findings suggest that ballast, as a coarse and highly permeable granular material, is susceptible to comparable hydraulic forcing, particularly when flow concentration occurs through structural gaps such as those between sleepers.

Recent numerical and physical model studies have advanced understanding of water flow through ballast, including the influence of fouling, permeability, and structural configuration (Tsubaki et al., 2017; Alrdadi & Meylan, 2022; Bian et al., 2016). However, few studies have systematically analyzed the complete breaching sequence and particle-scale dynamics under realistic railway configurations. The presence of sleepers, in particular, introduces both structural resistance and potential flow concentration points, potentially altering breach initiation timing and progression rate.

This study addresses this gap through reduced-scale physical modeling of ballasted railway embankments with a sleeper installed, tested under two flood intensities: 30 m³/h and 40 m³/h. Using a laboratory open-channel flume, seepage and overtopping-induced breaching were observed, and ballast particle movements were quantified via Particle Image Velocimetry (PIV). The aim is to compare failure mechanisms and failure times between the two discharges, providing experimental evidence for how hydraulic intensity influences breach mode and progression in sleeper-installed railway ballast layers.

2 MATERIAL AND EXPERIMENT SETUP

2.1 *Material*

The railway ballast used in this study was sourced from a quarry in northern Thailand. Its particle size distribution (PSD) was determined through laboratory testing. The results indicated that the ballast met the relevant standards and specifications, as illustrated in Figure 1. The measured bulk density of the ballast was 1,650 kg/m². Following the PSD verification, the ballast was scaled down to a 1:2 ratio for the purpose of constructing the physical model, taking into account both laboratory conditions and prototype characteristics. The PSD of the scaled-down 1:2 ballast is presented in Figure 2.

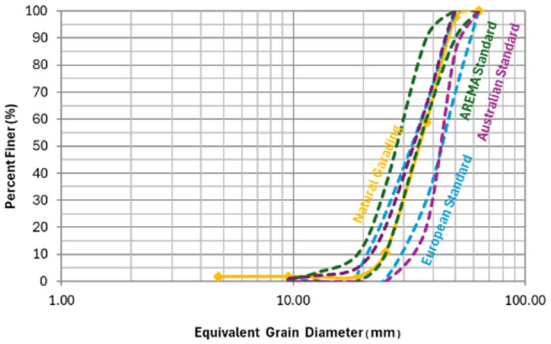

Figure 1 Particle size distribution of the tested railway ballast

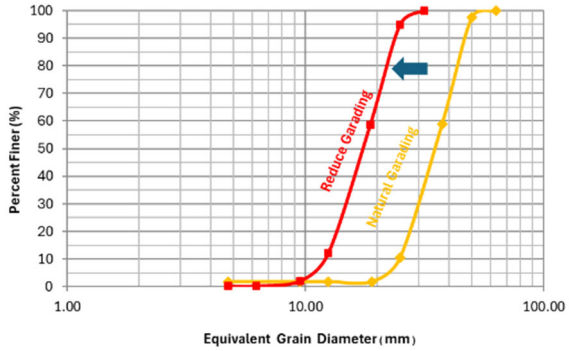

Figure 2 Particle size distribution of the 1:2 scaled railway ballast

2.2 *Experimental setup*

The flow-through testing of the ballast layer cross-section, simulating flood conditions, was conducted in an open-channel flume using a physical model test. The ballast material and the railway track geometry were scaled down at a ratio of 1:2, determined based on both the prototype and laboratory conditions.

For the preparation of the physical model, standard fresh ballast was used after it had undergone engineering property tests. The obtained engineering properties served as the basis for constructing the physical model. The geometry of the ballast track structure was designed in accordance with the Thai railway track design standards (Office of Transport and Traffic Policy and Planning, 2018) and was subsequently reduced to a 1:2 scale, as illustrated in Figure 2. The ballast particle size was determined based on the sieve analysis results of the standard fresh ballast and was then scaled down at a ratio of 1:2, as shown in Figure 3.

In the open-channel flume test, the preparation began by ensuring that the open-channel flume was ready for ballast installation. Ballast was then placed into the flume and compacted every 5 cm of height to achieve the required density. When the ballast height reached 15 cm, the sleeper was carefully positioned to ensure accurate placement. Ballast was then added and compacted every 5 cm until the total height reached 25 cm. The process of ballast installation are shown in Figure 4.

After the ballast placement and compaction were completed, the rail was installed on top of the prepared ballast structure. Finally, the ballast layer was checked for uniformity and density, and the stability of the sleeper and rail was verified before starting the test.

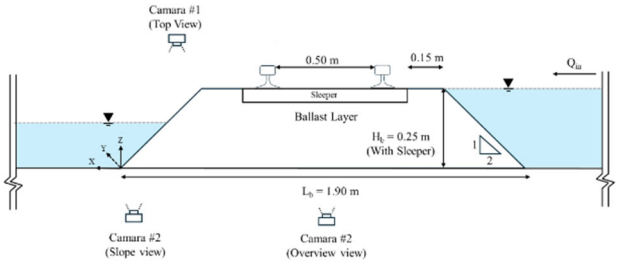

Figure 3 Schematic diagram of the experimental setup

Figure 4 Installation of the ballast in the open-channel flume

Figure 5 Installed ballast specimen in the open-channel flume before testing

2.3 *Procedure*

The open-channel flume used in this study had a total length of 10 m, a cross-sectional width of 309 mm, and a height of 450 mm. The flow-through tests were conducted on a ballast layer with a single sleeper at discharge rates of 30 m³/h and 40 m³/h to simulate different flood intensities. The tests continued until there was no further indication of additional ballast failure.

To record and analyze the ballast failure mechanisms in detail, three cameras were installed at different positions around the test area, as shown in Figure 3. The first camera was positioned above the flume to capture a top view, enabling observation of surface erosion and ballast particle movement. The second camera was installed to record longitudinal changes along the flume, allowing the assessment of ballast behavior during testing. The third camera was placed at the side to capture a lateral view, enabling detailed observation of the deformation of the ballast slope profile.

3 EXPERIMENTAL RESULTS

Two physical model tests were conducted to investigate the failure of ballasted railway embankments with a sleeper installed under discharge rates of 30 m³/h and 40 m³/h.

Figure 6 Ballast specimen in the open-channel flume after testing (30 m³/h)

Figure 7 Ballast specimen in the open-channel flume after testing (40 m³/h)

In the 30 m³/h test, the ballast embankment experienced a multi-phase retrogressive collapse. The ballast specimen after testing, shown in Figure 6, exhibited notable slope deformation, with ballast displaced from the crest toward the toe. The sleeper was partially exposed, indicating significant loss of supporting

material beneath and around its position. Ballast transported downslope accumulated at the toe, forming a sediment wedge as a result of the breach process. Seepage line development during testing (Figure 8) showed initial emergence at the downstream toe, producing a distinct wetting front along the slope face. As the test progressed, seepage concentrated beneath and between sleeper gaps, generating localized hydraulic jets that intensified scour in these zones. This focused erosion weakened the mid-slope region and promoted upslope migration of the failure zone. Failure began with toe instability at approximately 93 seconds, followed by progressive upslope displacement between 110 and 149 seconds. Overtopping occurred at 162 seconds, accelerating erosion, exposing the sleeper, and triggering a second slope collapse by 198 seconds. Final stabilization was reached between 310 and 324 seconds when no further movement was observed.

In the 40 m³/h test, failure occurred more rapidly and aggressively. The ballast specimen after testing (Figure 7) displayed severe slope retreat, with the sleeper fully exposed and a pronounced loss of ballast from both the crest and mid-slope areas. Accumulated deposits were evident at the downstream toe. Seepage observations (Figure 9) indicated early emergence between 71 and 97 seconds, with concentrated flow paths forming beneath and between sleeper gaps. Overtopping began at 121 seconds, producing high-velocity scouring along the slope face. A steep scarp formed and migrated upslope in a headcut pattern, removing large volumes of ballast in a short time. The breach widened and deepened rapidly, with full development completed by 168 seconds, after which no significant structural deformation occurred.

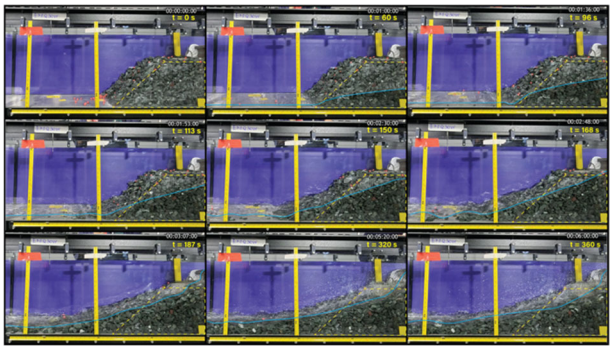

Figure 8 Seepage line in the ballast specimen during testing at a discharge rate of 30 m³/h

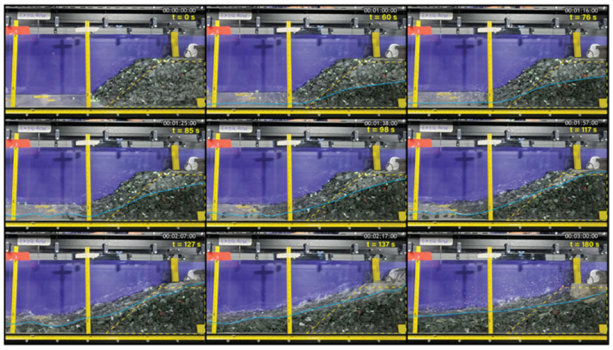

Figure 9 Seepage line in the ballast specimen during testing at a discharge rate of 40 m³/h

4 DISCUSSION

PIV analysis was employed to quantify the velocity magnitude of ballast particle movement during the two test cases: 30 m³/h and 40 m³/h. The resulting displacement and velocity fields provide detailed insights into how hydraulic loading and sleeper configuration influenced failure initiation and progression.

In the 30 m³/h case (Figure 10), ballast movement initiated at the downstream toe with relatively low velocity magnitudes, indicating a gradual destabilization phase. The displacement zone expanded upslope over time, with notable increases in velocity magnitude following overtopping at 162 seconds. The most intense movement occurred between sleeper gaps, where concentrated flow accelerated particle displacement during the second phase of failure. The breach developed through a multi-phase retrogressive collapse, with the overall failure process completing in approximately 310–324 seconds.

In contrast, the 40 m³/h case (Figure 11) displayed a markedly different velocity pattern. High-magnitude particle movement appeared much earlier, with localized zones of intense displacement forming between 71 and 97 seconds during the initial seepage and toe instability phase. Once overtopping began at 121 seconds, velocity magnitudes rapidly increased across a larger portion of the slope. The breach evolved into a headcut failure, with rapid upslope migration of the scarp and complete breach development by 168 seconds—approximately half the time required in the 30 m³/h test.

The comparison indicates that while both cases initiated failure at the downstream toe and progressed upslope, the higher discharge rate significantly reduced failure time and intensified the magnitude of particle movement from the early stages. The 30 m³/h case allowed for a more gradual progression, enabling the formation of multiple displacement phases, whereas the 40 m³/h case transitioned quickly to a single dominant failure phase dominated by high-velocity headcut erosion. These findings confirm that discharge intensity not only dictates the timing of breach formation but also shifts the prevailing failure mechanism from multi-phase retrogressive collapse to rapid headcut-driven breach.

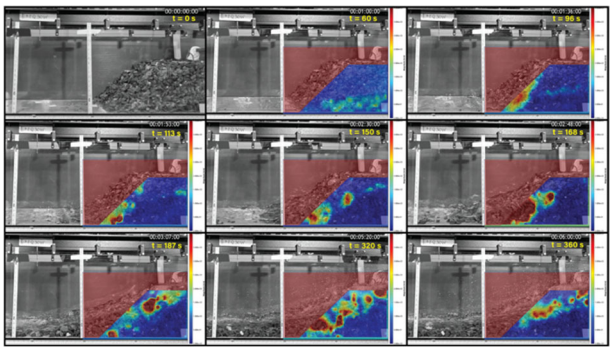

Figure 10 PIV analysis of the velocity magnitude during the test at a discharge rate of 30 m³/h

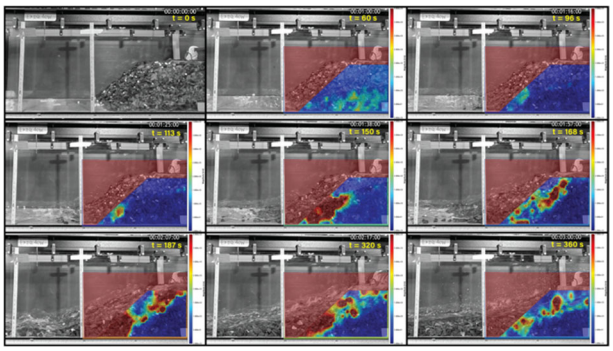

Figure 11 PIV analysis of the velocity magnitude during the test at a discharge rate of 40 m³/h

5 CONCLUSIONS

In conclusion, the physical model tests demonstrated that discharge rate strongly influences both the timing and mechanism of ballast embankment failure in the presence of a sleeper. The 30 m³/h case progressed through a slower, multi-phase retrogressive collapse, whereas the 40 m³/h case developed into a rapid headcut breach. PIV analysis further revealed that higher discharge produced earlier, more widespread, and higher-magnitude ballast particle movement, while moderate discharge allowed a more gradual progression with localized displacement concentrated between sleeper gaps.

- Both cases began with failure at the downstream toe, where seepage concentrated beneath and between sleeper gaps, triggering scour and promoting upslope migration of the failure zone.
- At 30 m³/h, breach development followed a multi-phase retrogressive collapse, with overtopping at 162 seconds and full failure after approximately 310 to 324 seconds. At 40 m³/h, the breach evolved into a rapid headcut-driven failure, with overtopping at 121 seconds and complete breach development by 168 seconds.
- Velocity magnitude analysis indicated that the 30 m³/h case experienced gradual particle mobilization, with the most significant displacement occurring between sleeper gaps during later stages. In contrast, the 40 m³/h case showed early and intense movement across a broader slope area, reflecting more aggressive erosion under higher hydraulic loading.
- Increasing discharge rate shortened failure time and shifted the dominant mechanism from staged retrogressive collapse to rapid headcut erosion, amplifying both the speed and magnitude of ballast particle displacement.

These findings highlight the critical influence of discharge intensity on breach evolution in sleeper-installed ballast embankments under flooding and demonstrate the utility of PIV analysis for capturing particle-scale dynamics in such failures.

6 ACKNOWLEDGEMENTS

The authors would like to extend their gratitude and acknowledge Chiang Mai University through the research and innovation research support scheme of Fundamental Funds (FF67/005) Grant No. 4707827 for the financial support.

7 REFERENCES

Alrdadi, R., and Meylan, M.H. 2022. Modelling water flow through railway ballast with random permeability and a free boundary. *Applied Mathematical Modelling* 103, 36–50.

Bian, X., Jiang, H., and Chen, Y. 2016. Preliminary Testing on High-speed Railway Substructure Due to Water Level Changes. *Procedia Engineering* 143, 769–781.

Johnston, I., Murphy, W., and Holden, J. 2024. The effects of internal erosion on granular soils used in transport embankments. *Soils and Foundations* 64.

Li, Y., Tian, C., Wen, L., Chen, A., Wang, L., and Qiu, W. 2021. A study of the overtopping breach of a sand-gravel embankment dam using experimental models. *Engineering Failure Analysis* 124.

Liu, G., Zhao, M., Liu, K., Connolly, D.P., Jiang, X., and Zhang, L. 2023. Comparative study of wicking and conventional railway geotextiles under flooding. *Construction and Building Materials* 400.

Polemio, M., and Lollino, P. 2011. Failure of infrastructure embankments induced by flooding and seepage: A neglected source of hazard. *Natural Hazards and Earth System Science* 11, 3383–3396.

Selig, E.T., and Waters, J.M. 1994. *Track Geotechnology and Substructure Management*. Thomas Telford Publishing.

Shen, D., Shi, Z., Zheng, H., Yang, J., and Hanley, K.J. 2022. Effects of grain composition on stability and breach process of landslide dams. *Geomorphology* 413.

State Railway of Thailand (SRT). 2021. Annual report.

Tsubaki, R., Kawahara, Y., and Ueda, Y. 2017. Railway embankment failure due to ballast layer breach caused by inundation flows. *Natural Hazards* 87, 717–738.

Zhou, G.G.D., Zhou, M., Shrestha, M.S., Song, D., Choi, C.E., and Cui, K.F.E. 2019. Experimental investigation on the longitudinal evolution of landslide dam breaching and outburst floods. *Geomorphology* 334, 29–43.

Zhao, C., Gao, Z., Luo, Z., Bian, X., and Chen, Y. 2024. Geogrid stabilization in ballasted trackbed for high-speed railways. *Transportation Geotechnics* 48, 101314.

Alrdadi, R., and Meylan, M.H. 2022. Modelling experimental measurements of fluid flow through railway ballast. *Fluids* 7.

Bian, X., Jiang, H., Chen, Y., and Han, J. 2015. Impact of water level rise on the behaviors of railway track structure and substructure: Full-scale experimental investigation. *Transportation Research Record* 2476, 15–22.

Hasnayn, M.M., McCarter, W.J., Woodward, P.K., Connolly, D.P., and Starrs, G. 2017. Railway subgrade performance during flooding and recovery. *Transportation Geotechnics* 11, 57–68.